Effects of bedding on the dynamic indirect tensile strength of coal: Laboratory experiments and numerical simulation

Yixin Zhao [a,b,c], Gao-Feng Zhao [d,*], Yaodong Jiang [a], Derek Elsworth [c], Yaqiong Huang [a]

[a] State Key Laboratory of Coal Resources and Safe Mining, China University of Mining and Technology, Beijing 100083, China
[b] College of Resources & Safety Engineering, China University of Mining and Technology, Beijing 100083, China
[c] Energy and Mineral Engineering, G³ Center and EMS Energy Institute, Pennsylvania State University, University Park, PA 16802, USA
[d] School of Civil and Environmental Engineering, The University of New South Wales, Sydney, NSW 2052, Australia

ARTICLE INFO

ABSTRACT

Dynamic indirect tensile tests were carried out by using a Split Hopkinson Pressure Bar (SHPB) for coal sampled from the Datong mine in China. The principal purpose was to explore the influence of bedding structure in the coal on its dynamic indirect tensile strength. However, to resolve some contradictions, X-ray micro CT, high speed optical imaging and a discrete element based modelling approach were combined to analyze the test results. The X-ray micro CT was used to detect the actual bedding structure in the coal; the high speed imaging captured failure patterns of the specimens with different bedding directions; and the numerical modelling was utilized to investigate the influence of different bedding structures on dynamic strength. The SHPB and numerical results illustrate that dynamic indirect tensile strength reliably correlates with impact velocity. In addition, the dynamic indirect tensile strength is not only influenced by the bedding direction but also by the roughness and discontinuity of the bedding. Based on these findings, a method is developed to further process the test data including a model to describe the dynamic indirect tensile strength of Datong coal.

© 2014 Elsevier B.V. All rights reserved.

1. Introduction

The dynamic mechanical properties of coal are of great importance in coal mining engineering where they relate to the selection of blasting parameters, stability analysis of coal roadways under impact loading, and the prevention of coal bumps and bursts. Related research on dynamic mechanical properties of coal has been conducted since the 1950s. For example, Morgans and Terry (1958) reported on the static and dynamic elastic modulus of coal, Szwilski (1984) measured the anisotropic elastic modulus of coal, and Morcote et al. (2010) conducted ultrasonic tests to study the dynamic elastic properties of coal. In addition, the elastic properties and the failure of coal under dynamic loading conditions have also been studied, e.g. the mixed-mode fracture toughness of coal (Zipf and Bieniawski, 1990), the dynamic compressive and tensile strength of coal (Xia et al., 2010), and the mode-I fracturing of coal under impact loading (Zhao et al., 2013b). Among these, the dynamic tensile strength is one of the most common features and the most used of the index properties of coals for their dynamic characterization. To quantify the dynamic tensile strength of coal, direct tensile and indirect tensile testing methods can be used. For example, Okubo et al. (2006) reported the dynamic tensile strength of Beijing coal by using

the direct tensile testing method and Xia et al. (2010) performed dynamic indirect tensile tests on a number of coal samples from mines of India. However, direct tensile tests are very difficult and complicated to perform (Zhang and Zhao, 2013). Thus, researchers developed several indirect tensile testing methods, such as the Brazilian disc (BD), bending and spalling methods. Among them, the BD specimen in the split Hopkinson pressure bar (SHPB) system is widely employed to achieve the dynamic tensile strength of coal or rock (Zhang and Zhao, 2013). The indirect BD methods provide a convenient means of conducting tests in terms of specimen manufacturing, experimental setup and data reduction, but the complex networks of bedding planes in coals result in difficulties to characterize the dynamic features of coals. Moreover, previous research has been more focused on the macroscopic mechanical response and the influence of the bedding structure on the dynamic tensile failure of coal remains unclear. Thus, the understanding of the contribution of bedding structures on dynamic tensile failure of coal is both important and necessary.

In this study, a number of dynamic indirect tensile tests for Datong coal are conducted by using an SHPB. It focuses on the influence of the bedding structure on the dynamic indirect tensile strength of Datong coal. Coal specimens with different bedding direction (along the loading direction) were tested by using the SHPB under different impact velocities. Before the test, the density and dynamic elastic modulus were measured. To further define the influence of bedding structure, X-ray micro CT is used to provide spatial data to inform the meshing of

* Corresponding author. Tel.: +61 2 9385 6139; fax: +61 2 9385 5022.
E-mail address: gaofeng.zhao@unsw.edu.au (G.-F. Zhao).

discrete element-based numerical models to investigate the influence of different bedding structures on the dynamic tensile failure of coal. From comparison between the experimental and numerical results, relationships are developed to describe the dynamic indirect tensile strength for Datong coal as a function of impact energy.

2. Experimental setup

2.1. Specimen preparation

A total of 45 specimens were cut from a single block from the working face of the Xinzhouyao coal mine in Datong, China. According to the ISRM suggested method (Zhou et al., 2012), the diameter and height of these specimens were 50 mm and 25 mm, respectively (see Fig. 1a). The actual dimensions of these specimens are listed in Table 1, which are slightly different from these design values due to the errors induced by the manufacturing operation. The two ends of these specimens were ground to parallel within 0.05 mm and perpendicular to the longitudinal axis within 0.25°.

2.2. Characteristics of coal samples

The selected coal samples from the No. 11 seam of the Xinzhouyao coal mine are bituminous coals, with vitrinite reflectance (R_o) of 0.76–0.85%. The moisture content (4.0%), ash (2.3%), volatile matter (25.0%) and fixed carbon (68.7%) were determined by proximate analysis (ASTM D5142, 2009). The average maceral composition consists of an abundant vitrinite group (75.4%), mainly comprising telocollinite (11.0%), telinite (41.2%), desmocollinite (19.5%), and corpocollinite (3.7%). The inertinite group (20.0%) is essentially composed of semifusinite (10.2%), fusinite (5.3%), inertodetrinite (4.3%) and macrinite (0.2%). Minor amounts of the liptinite group (1.8%) have also been observed. Mineral matter is generally poorly presented (2.6%), which consists of pyrite (2.2%), clay minerals (0.2%) and carbonate minerals (0.2%).

Table 1 summarized the density and the dynamic elastic modulus of 45 prepared specimens. The NM-3C ultrasonic non-metal analyzer was applied to obtain the dynamic elastic modulus of coal specimens before the SHPB tests. The dynamic elastic modulus is tested along the designed impact direction. Since ultrasonic test was performed in the elastic range, there was no any damage or plastic deformation occurred in
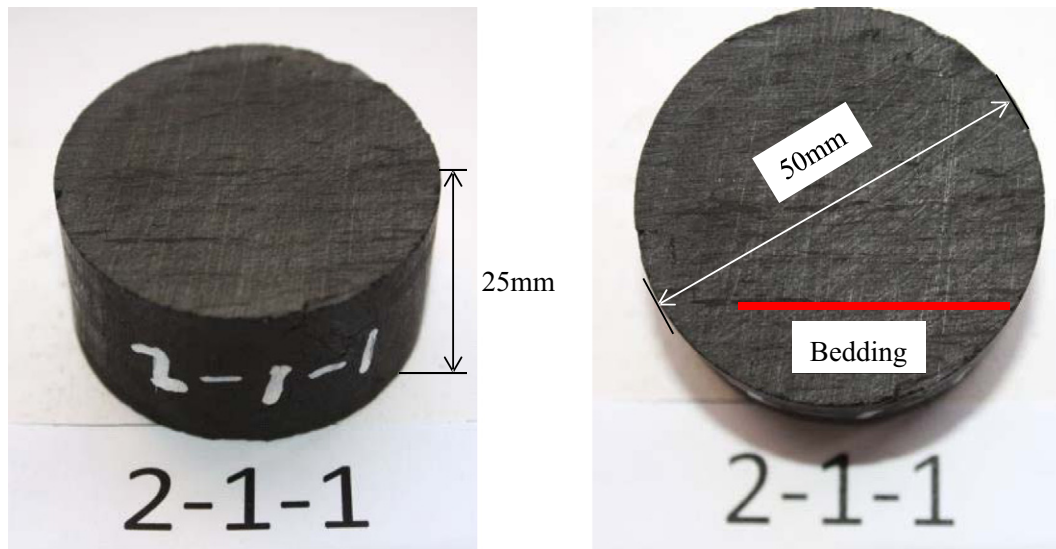
(a) Coal specimen
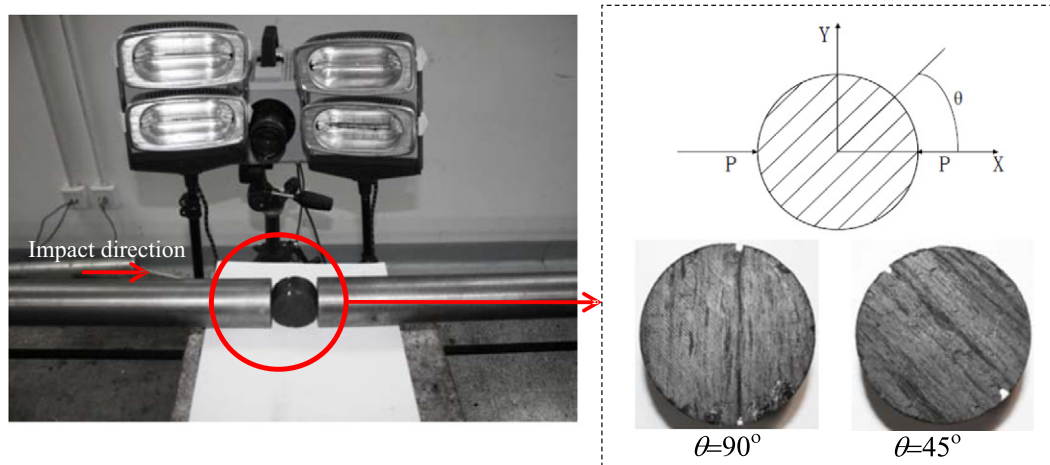
(b) Setup of the SHPB test

Fig. 1. BD specimen and the test setup of the dynamic indirect tensile test.

Table 1
Dimension, density and dynamic elastic modulus of 45 coal specimens prepared for the dynamic indirect tensile test.

Specimen ID	Bedding direction (°)	Diameter (mm)	Height (mm)	Density ($10^3 \times$ kg/m³)	Elastic modulus (GPa)
111	0.0	49.22	24.62	1.31	2.91
112	0.0	49.42	25.30	1.31	2.78
113	0.0	49.42	25.90	1.32	2.72
211	0.0	49.40	25.40	1.30	2.55
212	0.0	49.40	25.70	1.31	2.68
213	0.0	49.12	25.10	1.33	2.40
421	0.0	49.32	25.58	1.29	2.20
422	0.0	49.35	25.10	1.30	2.01
423	0.0	49.20	24.70	1.29	2.16
121	22.5	49.36	25.40	1.30	2.55
122	22.5	49.32	25.50	1.31	2.72
123	22.5	49.36	25.68	1.33	2.45
231	22.5	49.26	25.54	1.33	2.33
232	22.5	49.20	25.30	1.33	2.42
233	22.5	49.28	24.80	1.32	2.48
451	22.5	49.20	25.02	1.37	2.32
452	22.5	49.30	25.72	1.29	2.31
453	22.5	49.40	25.80	1.30	2.26
161	45.0	49.26	25.08	1.31	2.30
162	45.0	49.32	25.90	1.31	2.43
163	45.0	49.40	25.70	1.32	2.63
3111	45.0	49.30	25.50	1.37	2.44
3112	45.0	49.30	25.80	1.35	2.17
3113	45.0	49.40	25.10	1.36	2.41
471	45.0	49.20	25.90	1.29	2.03
472	45.0	49.30	25.78	1.30	2.42
473	45.0	49.36	25.36	1.28	2.36
164	67.5	49.38	25.50	1.33	2.66
165	67.5	49.44	25.20	1.31	2.40
151	67.5	49.26	24.82	1.35	3.09
361	67.5	49.22	25.28	1.32	2.13
362	67.5	49.30	25.48	1.32	1.87
363	67.5	49.28	25.14	1.31	2.18
481	67.5	49.40	25.60	1.27	3.01
482	67.5	49.32	24.80	1.42	2.27
483	67.5	49.22	23.80	1.29	2.87
141	90.0	49.42	25.54	1.32	1.89
142	90.0	49.32	25.00	1.31	2.31
143	90.0	49.22	25.70	1.33	2.44
411	90.0	49.20	25.48	1.30	2.16
412	90.0	49.26	25.08	1.29	1.98
413	90.0	49.28	25.70	1.29	1.98
491	90.0	49.32	25.00	1.29	2.11
492	90.0	49.32	25.70	1.30	2.21
493	90.0	49.32	25.70	1.29	2.03

Table 2
Final results of the dynamic indirect tensile test on 32 coal specimens.

Specimen ID	Bedding direction (o)	Impact velocity (m/s)	Strain rate (s^{-1})	Failure time (μs)	Dynamic indirect tensile strength (MPa)
421	0.0	2.701	55.827	130	4.272
211	0.0	3.213	54.855	130	4.942
112	0.0	3.328	58.947	139	4.998
113	0.0	3.487	73.735	129	5.113
212	0.0	3.565	74.326	161	5.263
122	22.5	2.378	54.758	133	4.001
232	22.5	2.518	56.103	177	4.206
233	22.5	2.565	56.194	172	4.301
452	22.5	2.972	54.327	170	4.587
121	22.5	3.298	63.848	156	5.100
453	22.5	3.803	72.446	120	5.441
161	45.0	2.624	49.389	165	4.583
162	45.0	3.146	58.824	141	5.011
472	45.0	3.226	58.118	119	5.193
471	45.0	3.768	68.421	116	5.709
3111	45.0	3.882	75.594	123	5.905
3113	45.0	3.884	95.895	138	5.917
481	67.5	2.125	39.395	124	3.730
482	67.5	2.689	52.053	127	4.380
151	67.5	3.286	65.897	135	5.375
363	67.5	3.332	60.992	108	5.306
362	67.5	3.448	72.750	130	5.405
165	67.5	3.689	73.390	131	5.409
164	67.5	3.703	73.565	189	5.507
361	67.5	4.008	79.009	162	5.733
491	90.0	2.105	40.747	121	3.893
492	90.0	2.113	37.776	160	3.897
412	90.0	2.336	41.466	181	3.923
411	90.0	2.779	50.390	157	4.862
413	90.0	2.970	54.737	206	4.862
493	90.0	3.018	52.237	194	5.051
143	90.0	3.843	73.487	147	5.860

$P(t)$ and displacement $U(t)$ is calculated using the following equations:

$$P(t) = EA \frac{(\varepsilon_I(t) + \varepsilon_R(t) + \varepsilon_T(t))}{2} \tag{1}$$

$$U(t) = C \int_0^t (\varepsilon_I(t) - \varepsilon_R(t) - \varepsilon_T(t)) \tag{2}$$

where E is the elastic modulus of the incident (transmission) bar (200 GPa), A is the cross sectional area of the incident (transmission) bar, and C is the one dimensional longitudinal stress wave velocity in the incident (transmission) bar. The indirect tensile strength of the coal specimen is obtained as

$$\sigma_t = \frac{2P_{\max}}{\pi DL} \tag{3}$$

where L is the thickness of the coal specimen (25 mm), D is the diameter of the coal specimen (50 mm), and $P_{\max}$ is the maximum value of the loading force, $P(t)$.

The strain rate of the coal specimen which reflects the loading condition of the SHPB test is

$$\dot{\varepsilon}(t) = C(\varepsilon_I(t) - \varepsilon_R(t) - \varepsilon_T(t)). \tag{4}$$

Another common index used to reflect the dynamic loading condition in the dynamic indirect tensile strength recovered from the SHPB is the loading rate, which can be obtained as

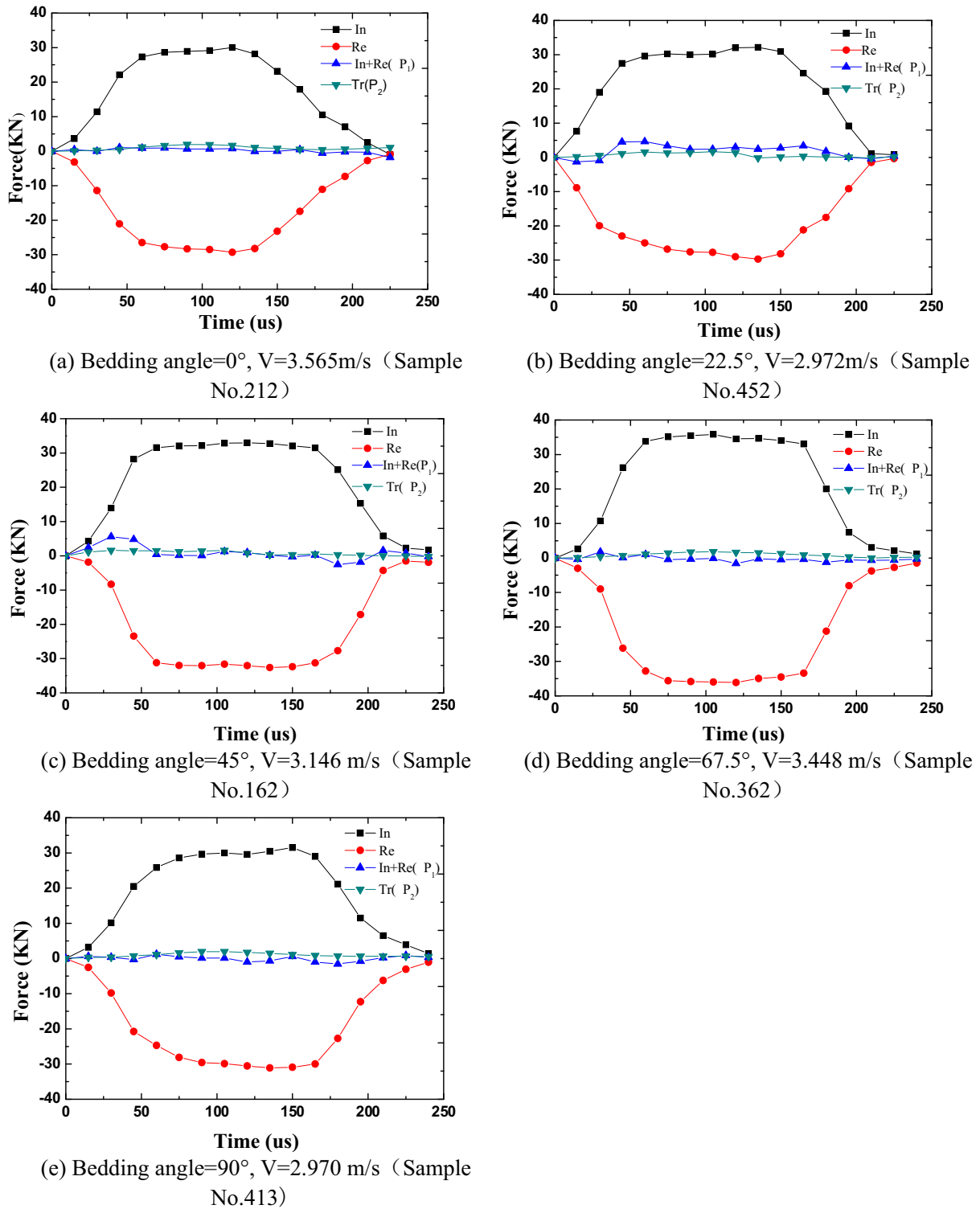$$\dot{\sigma}_t = \frac{\sigma_t}{t_d} \tag{5}$$

the coal specimen. The detailed information about the ultrasonic test can be found in the related article (Morcote et al., 2010).

2.3. Split Hopkinson Pressure Bar (SHPB) test

The SHPB is located at the State Key Lab for Geomechanics and Deep Underground Engineering of CUMTB. It comprises a gas gun, a cylindrical steel striker bar (50 mm in diameter and 400 mm in length), an incident bar (50 mm in diameter and 2000 mm in length), and a transmission bar (50 mm in diameter and 2000 mm in length). The setup of the dynamic indirect tensile test using the SHPB is illustrated in Fig. 1b, in which the coal specimen is placed between the incident bar and transmission bar. During the test, the striker bar is launched by the gas gun at high speed to impact the incident bar. The resulting strain wave $\varepsilon_I(t)$ is of short duration, is reflected at the interface between the specimen and incidental bar and is recorded both as a reflected strain wave $\varepsilon_R(t)$, and as a transmitted strain wave $\varepsilon_T(t)$. The characteristics of these strain waves are obtained from two dynamic strain gauges mounted on each the incident bar and transmission bar. Then, the loading force

(a) Bedding angle=0°, V=3.565m/s（Sample No.212）

(b) Bedding angle=22.5°, V=2.972m/s（Sample No.452）

(c) Bedding angle=45°, V=3.146 m/s（Sample No.162）

(d) Bedding angle=67.5°, V=3.448 m/s（Sample No.362）

(e) Bedding angle=90°, V=2.970 m/s（Sample No.413）

Fig. 2. Dynamic force balance check for six typical dynamic BD tests on the Datong coal.

where t_d is the time when the load $P(t)$ reaches its peak. More details on the dynamic indirect tensile test recovered from the SHPB can be found in the work of Dai et al. (2010). In this work, to investigate influence of the bedding structure on the dynamic indirect tensile strength of Datong coal, the bedding directions (angles between the bedding and loading directions) were varied from 0 to 90° with an interval of 22.5°. In addition, the dynamic elastic modulus of these specimens was obtained from ultrasonic tests before the destructive SHPB loading. The actual bedding structure of each coal specimen was recovered

from X-ray micro CT and failure patterns captured by high-speed digital photography.

3. Results and discussion

3.1. Test results

Only 32 of the 45 specimens were successfully tested for dynamic in-direct tensile strength in the SHPB experiments. Table 2 lists the impact

(a) Density
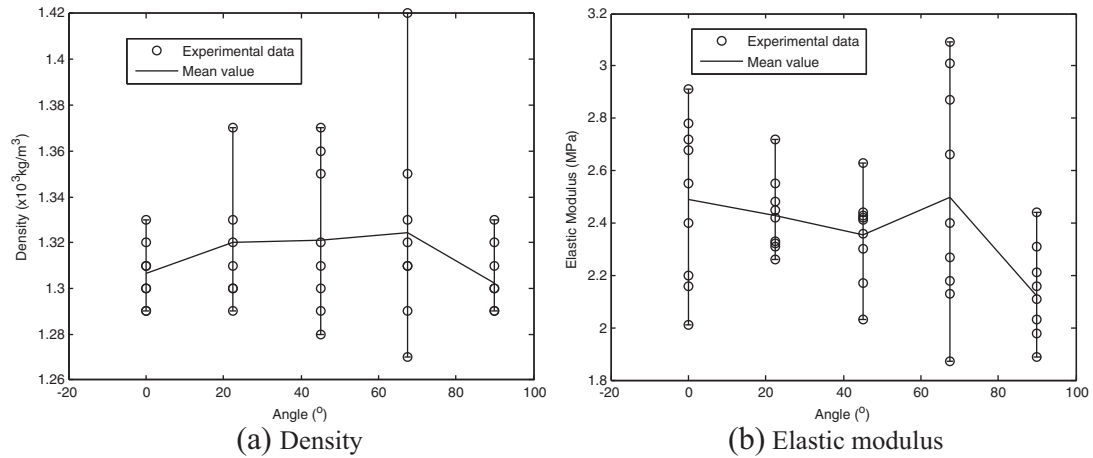
(b) Elastic modulus

Fig. 3. Density and dynamic elastic modulus of Datong coal specimens with different bedding directions.

velocity, the strain rate, the loading rate and the dynamic indirect tensile strength of these SHPB tests. It should be mentioned that according to the ISRM suggested method (Zhou et al., 2012) dynamic force balance on all SHPB tests was checked and the results show that the condition was satisfied for all of the tests. Fig. 2 shows the results of dynamic force balance check for six typical dynamic BD tests on the Datong coal.

Fig. 3 shows the density and dynamic elastic modulus of these specimens versus the bedding direction. Density (Fig. 3a) is plotted for reference and to check the scatter in the dynamic modulus of those specimens since this scatter might obscure the true influence of bedding direction (see Fig. 3b). Density is directly related to the mass distribution (heterogeneity) of the specimen, and it should be invariant with the bedding direction. Therefore, the variation in density with bedding direction is used as a reference in verifying the utility of averaging dynamic elastic moduli. As expected, density (averaged value) is uncorrelated with bedding direction, whereas, an apparent correlation exists for the dynamic elastic modulus (average value). It is also observed that the difference between the individual specimen density and the average density is relatively small compared with that of the dynamic elastic modulus. Therefore, the density is reliable and nearly constant for different specimens. Moreover, from comparison between the scatter of the density and the dynamic elastic modulus of samples with the same bedding direction, it is apparent that the differences of these two properties are highly correlated, i.e. an usually higher variation of the density will result in a higher variation of the dynamic elastic modulus. Overall, the elastic response of Datong coal is anisotropic.

During the test, the load–displacement curves were recorded (see Fig. 4), which were further being used to calculate the corresponding indirect tensile strength by using Eq. (3). Analyses of dynamic indirect tensile strength of those coal specimens are shown in Fig. 5. These figures show relationships between the impact velocity, the strain rate and the loading rate and the dynamic indirect tensile strength. Besides magnitude of the indirect tensile strength, the dynamic effect, the gradient of the fitting line (see Fig. 5a to c), is another important index. Due to the crisp property of coal under impact loading, high strain rate can't be applied by using the SHPB. It was found that when strain rate is more than $0.9 \times 10^2 \, \mathrm{s}^{-1}$, the coal specimen will turn into a group of fragments and the dynamic force balance requirement cannot be satisfied. Thus, the obtained strain rate ranges for the Datong coal on an SHPB was only from 0.4×10^2 to $0.9 \times 10^2 \, \mathrm{s}^{-1}$. Equations to represent the dynamic strength of rock like materials can be a logarithmic function (Zhao, 2000) or a more

complex equation (Gong and Zhao, 2013). However, these nonlinear equations are applicable for test data with range of many order difference of the strain rate. For the Datong coal data, to directly use these high nonlinear functions is actually improper due to the strain rate range is too small. As we know, to use a high nonlinear function for global scale fitting test data of limited range the over shooting is unavoidable and might provide misunderstanding on the result. For a small range $(x, x + \mathrm{d}x)$, the linear function is the 1st order Taylor expansion for any complex nonlinear function, and is reasonable to be used as the regression function. Therefore, in the paper, the linear function was adopted to analyze the test data of Datong coal. From Fig. 5, the increase of dynamic indirect strength with loading rate of Datong coal was successfully captured. Fig. 5a indicates that the angle of bedding plane make less effect to the dynamic tensile strength of coal compared with the impact velocity. As the impact direction vertical to the bedding plane ($\theta = 90°$) and the impact velocity is larger than 3.1 m/s, the dynamic tensile strength of coal keeps larger than that of coal with other bedding angles based on the linear fit results. However, as the impact velocity is less than 3.1 m/s, the dynamic tensile strength of coal with the 45° bedding angle researches the highest. Nevertheless, the dynamic tensile strength of coal with the 22.5° bedding angle reaches to the lowest as the impact velocity larger than 3.6 m/s. But the dynamic tensile strength of coal with the 0° bedding angle is the lowest as the impact velocity less than 3.6 m/s.

In exploring the influence of bedding structure on the dynamic properties of Datong coal, some contradictions are apparent—i.e. the influences of bedding orientation on the dynamic effect obtained from Fig. 5a to c are quite different. The dynamic effect based on the impact velocity is nearly constant (see Fig. 5a). However, much scatter in results is apparent from the strain rate and loading rate (see Fig. 5b and c). It should be mentioned that the strain rate and loading rate are the most commonly-used independent variables in the SHPB test (Xia et al., 2010). In the following, this problem is addressed by numerical experimentation.

Due to the natural heterogeneous property of coal, the experimental data is so scatter that it is nearly impossible to capture the main influence tendency of the bedding even if a large number of tests were conducted. Moreover, in the SHPB test, there is only one controllable parameter that is the impact velocity. Other parameters, such as strain rate and loading rate, are derived parameters by using Eqs. (4) to (5) based on the assumption of 1D elastic stress wave propagation (Xia et al., 2010) which will generate some system error that might pollute the test data (strain rate and loading rate) as well. To tackle these
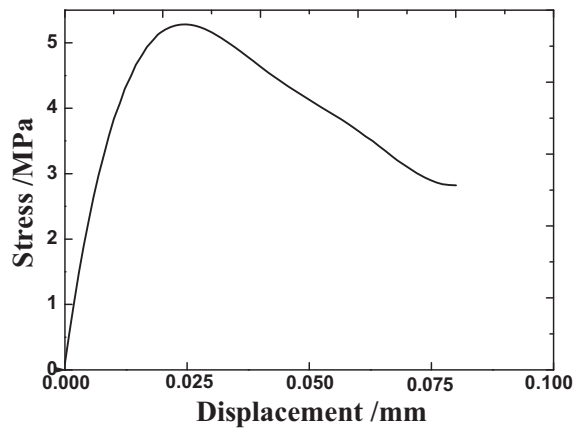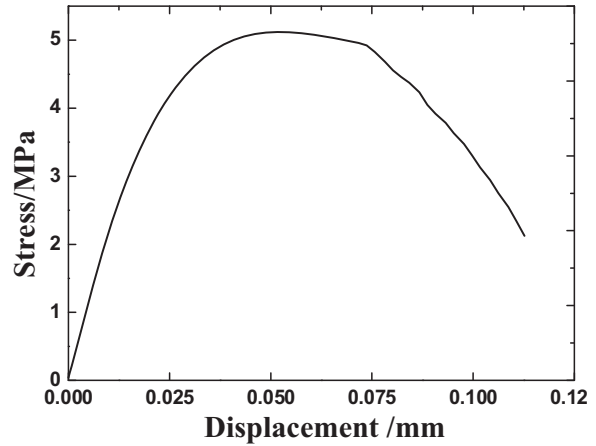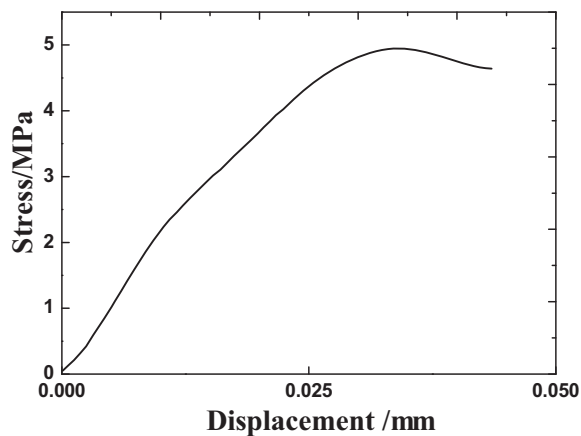
(a) Bedding angle=0°, V=3.565m/s（Sample No.212）
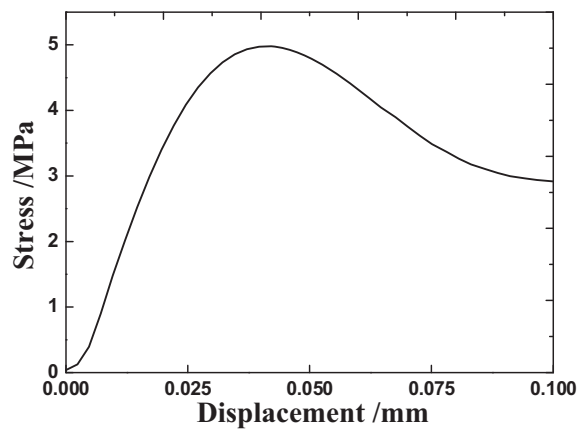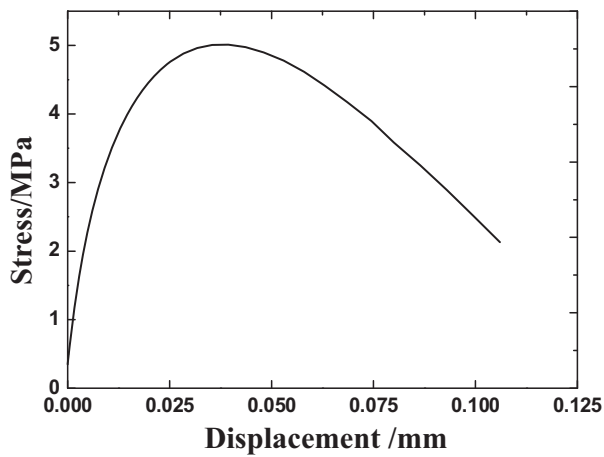
(b) Bedding angle=22.5°, V=2.972m/s（Sample No.452）

(c) Bedding angle=45°, V=3.146 m/s（Sample No.162）

(d) Bedding angle=67.5°, V=3.448 m/s（Sample No.362）

(e) Bedding angle=90°, V=2.970 m/s（Sample No.413）

Fig. 4. Stress and strain relationship of air dry Datong coals with various bedding angles under selected impacted velocity.

dilemmas, numerical simulation based on discrete element model was adopted to filter out the uncontrollable influence factors, e.g. heterogeneous natural of the coal specimen and system error of the SHPB test due to the 1D stress wave propagation assumption. For this reason, the detailed discussion on the test results will be conducted in the following section.

3.2. Numerical modelling

In this section, the Distinct Lattice Spring Model (DLSM) (Zhao, 2010; Zhao et al., 2011) is used as a numerical tool to further study the influence of bedding structure on the dynamic indirect tensile strength of Datong coal. Solution method of the DLSM is the same as
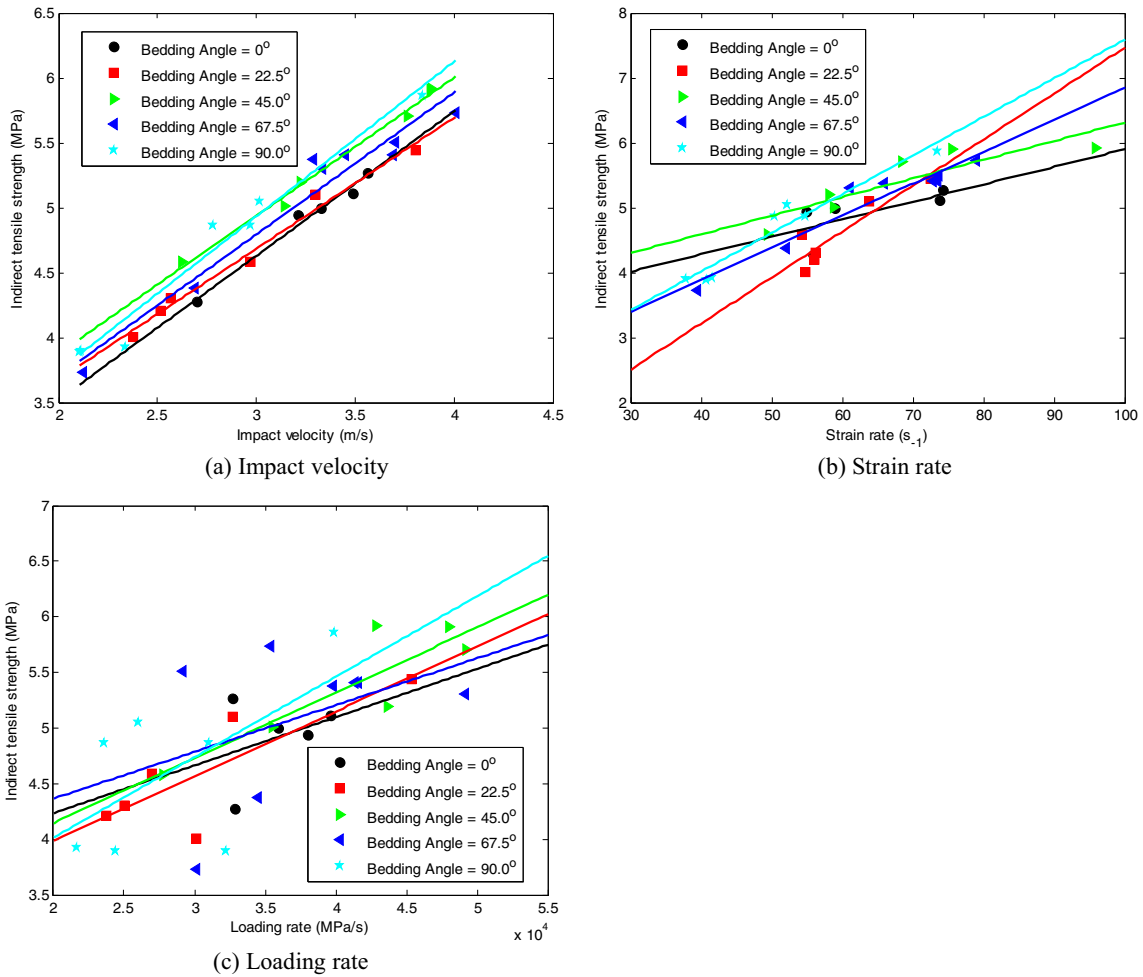
(a) Impact velocity

(b) Strain rate

(c) Loading rate

Fig. 5. Dynamic indirect tensile strength versus impact velocity, strain rate and loading rate for coal specimens with different bedding directions from the SHPB test.

the classical DEM. However, compared with classical Discrete Element Model (DEM), the DLSM has advantages on free of calibration of micro-mechanical parameters, easy to represent discontinuities and more computational efficient. The material is represented as a group of particles with different sizes connected by shear and normal springs. The utilization of shear spring allows the modeling of multi-body non-central interaction. The input parameters in the DLSM are the Young's modulus E and the Poisson's ratio ν. The spring stiffness is calculated

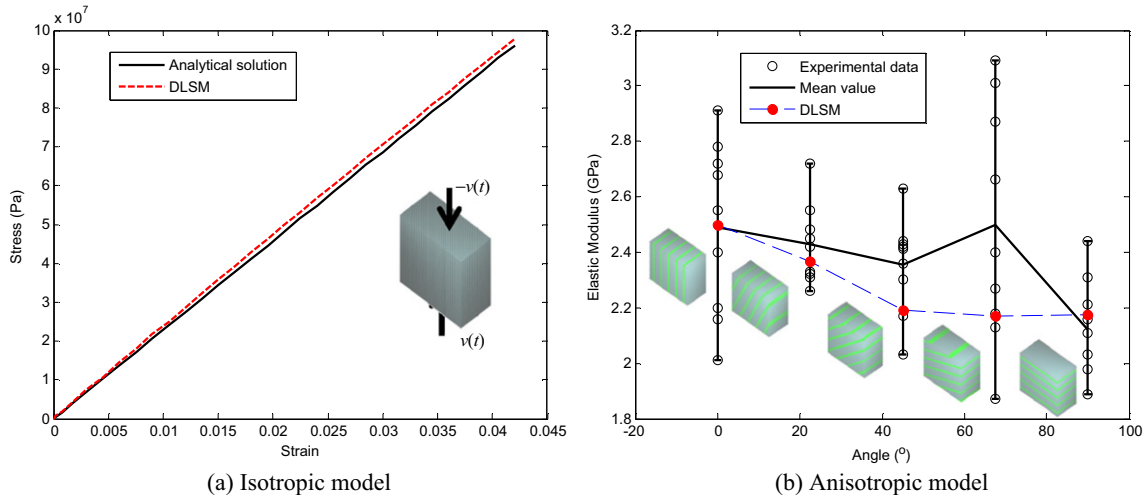(a) Isotropic model

(b) Anisotropic model

Fig. 6. Strain to stress curves predicted by the isotropic DLSM model and the elastic modulus predicted by using an anisotropic DLSM model.
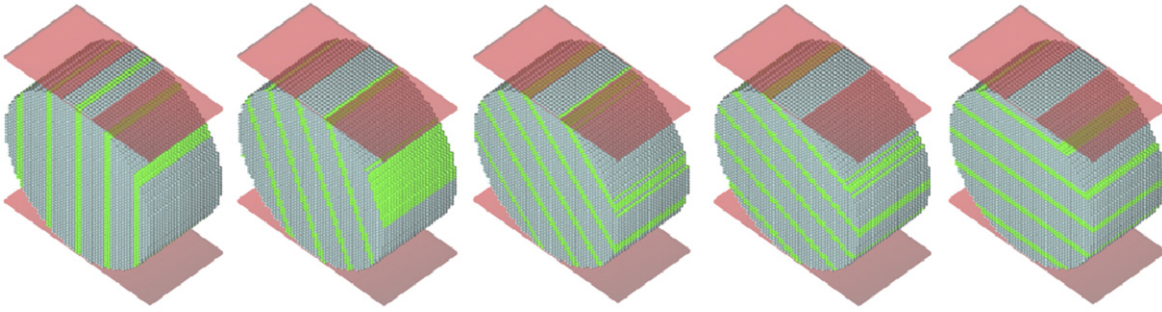
Fig 7. Computational models with bedding planes for the dynamic indirect tensile strength test simulated by using the DLSM.

by using a closed form equation (Zhao et al., 2011). Up to now, the DLSM have been successfully used in studies of dynamic cracking of brittle material (Kazerani et al., 2010), indirect tensile failure of Changsha sandstone (Gong and Zhao, 2013), stress wave propagation in jointed rock masses (Zhu et al., 2011), etc. A detailed review on the application and development of the DLSM can be found in Zhao and Zhao (2012).

In this paper, the DLSM was adopted as the numerical simulation tool for the following reasons. First, the DLSM is made up from the most basic ingredients, e.g. mass particles, Hooke springs, the Newton's second law, and a deformation based brittle failure criterion for the normal spring, there is no complex constitutive models adopted. Therefore, the numerical simulation results can be easily interpreted. For example, if we change the bedding angle, the numerical results would directly reflect this change rather than including the constitutive change caused by the bedding direction. Second, the meshless property of the DLSM also make the method is easy to build up complex models. Third, the high performance computing ability of the DLSM (Zhao et al., 2013a) make the parameter analysis more convince, e.g. around one hundred simulations were conducted for this paper. For above reasons, the DLSM was selected as the tool to investigate the influence of bedding structure (bedding angle, bedding roughness and bedding discontinuity) on the dynamic indirect tensile strength of the Datong coal.

3.2.1. Anisotropic elastic modulus

We simulate a uniaxial compression test on a 50 mm × 50 mm × 25 mm cube using DLSM. The particle size is 1 mm and the computational model comprises 62,500 particles. This model is used as the base model for the following sections. Computational models with different configurations of bedding structure are also built by using a texture mapping approach (Zhao et al., 2014). For the isotropic model, material parameters are selected as: Elastic modulus 2.29 GPa, Poisson ratio 0.23, and Density 1315 kg/m^3 (representative of Datong coal under isotropic assumption). In reality, cylindrical specimen with height to diameter ratio of two is usually adopted for uniaxial compression test. Here, we adopted the cube specimen for following reasons. First, in numerical simulation, the zero friction condition of two loading plates is satisfied. Therefore, there is no end effect. The second reason is to provide the base model for the further SHPB test, in which the disc specimen can be cut from the current calibrated model directly (see Fig. 6). The applicable of using a cube specimen in the DLSM simulation is also verified against the analytical solution. Fig. 6a shows the strain stress curves predicted by the numerical simulation (F/A, F is the reaction force of the model to the loading plate, A is the loading area of the specimen) and analytical solution ($E \times \varepsilon$, E is the input elastic modulus and ε is the model strain). It indicates that the particle size of the computational model (1 mm) can reasonably represent the isotropic elastic deformation of Datong coal.

As the bedding structure always reduces the cohesion of coal matrix, the bedding structure in Datong coal is represented as a group of thin

layers with weaker elastic modulus in the numerical modelling. The elastic parameters for the base and weak layer are obtained by using the empirical method described in You et al. (2011). In this work, the elastic modulus of the base model is calculated as 2.85 GPa, and that of the weak layer was 1.05 GPa. The remaining parameters are the same as these applied in the isotropic model. A total of five computational models are simulated. The elastic moduli are calculated from the corresponding strain–stress curves (e.g. Fig. 6). The final results are shown in Fig. 6b, indicating that the anisotropic response is successfully captured by the DLSM. This model is further applied to study the dynamic indirect tensile strength testing of coal.

3.2.2. Dynamic indirect tensile strength

Modeling was completed on BD specimens (see Fig. 7) accommodating different inclinations of bedding planes. The elastic parameters were taken as the same in the previous analyses with two further failure parameters, the threshold values of normal spring tensile failure for the base and layer, required to be recovered from calibration. These are determined from a comparison between the simulated dynamic indirect tensile strength and the corresponding experimental data where the bedding is horizontal. In the DLSM, the control parameter of tensile strength is the threshold value of the normal spring. For a given material, it can be obtained from a trial and error process, i.e. when the predicted strength is low then increase the threshold value, and vice versa. For the Datong coal, the threshold value for the bedding is firstly calibrated to let the fracture happen along the centre line. Since further reduce the value will not result the failure of the specimen. A further reduction on the threshold value of the base material is conducted to let the specimen's strength close to the experimental observation. In this study, these two parameters are obtained as 0.009 mm and 0.004 mm. As suggested by Ma et al. (2010), a step velocity loading with a rise time of 200 μs was used to mimic the loading condition of the dynamic indirect tensile strength for an SHPB. The numerical results are summarized in Fig. 8. The relationship showing an increase in dynamic indirect tensile strength with an increase in impact velocity is successfully reproduced in the numerical simulation. A similar tendency of the influence of bedding direction on the dynamic effect, as observed in the experimental results, is also obtained (see Fig. 8a). Moreover, unlike the SHPB data shown in Fig. 5, the overall trend of the influence of bedding direction on the dynamic indirect tensile strength in Fig. 8 was similarly recovered. It is concluded that the contradictions in the SHPB data result from the systematic errors introduced in the dynamic strain gauge data. This indicates that the differences in the dynamic effect caused by the bedding structure are small and can be ignored. Moreover, for the dynamic indirect tensile test conducted by using an SHPB, the impact velocity is recommended as the most essential data to be reported, which can be further used in the analysis of the experimental data. However, differences in the tensile strength resulting from bedding directions, as predicted by the DLSM, are much larger than those of the SHPB data (see Figs. 5 and 8).
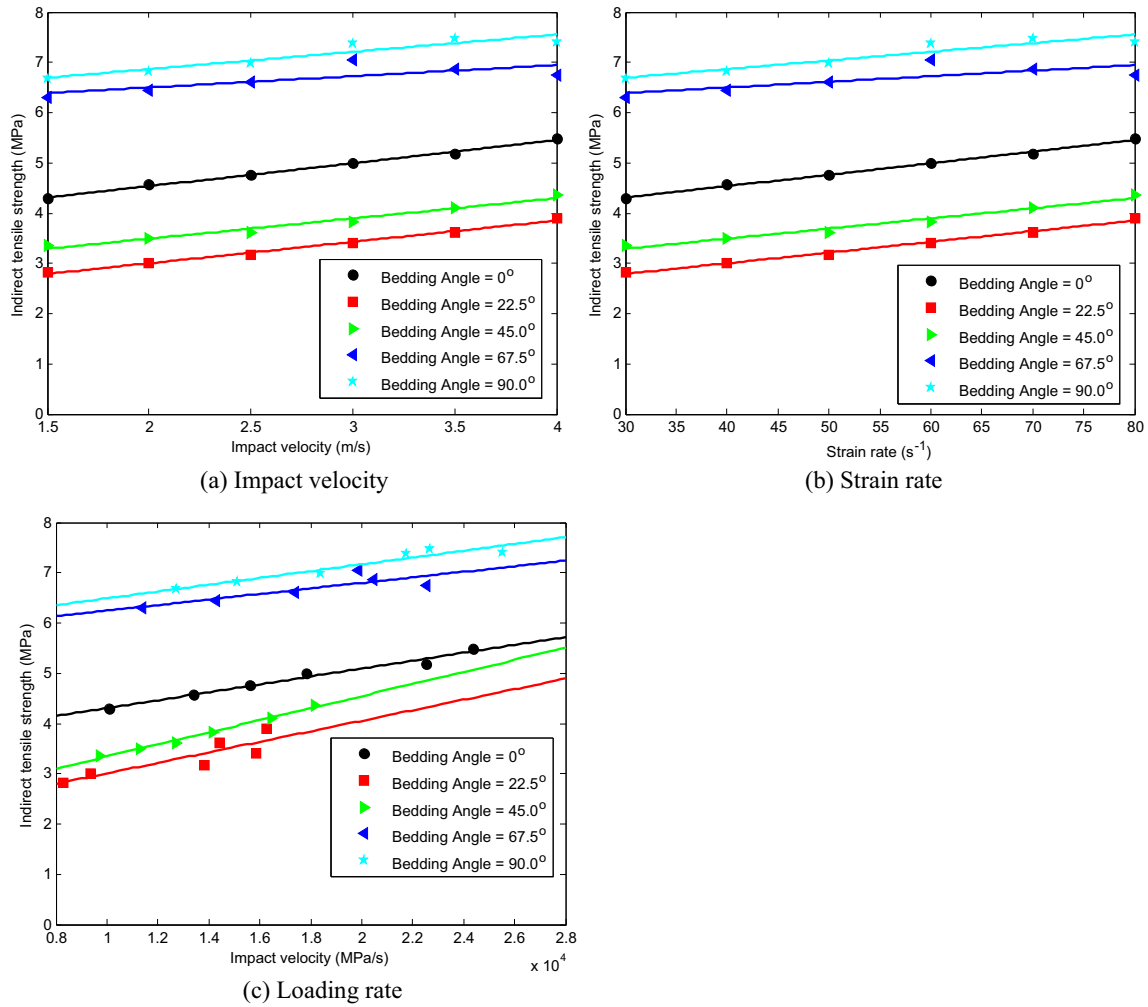
(a) Impact velocity

(b) Strain rate

(c) Loading rate

Fig. 8. Dynamic indirect tensile strength versus impact velocity, strain rate and loading rate for Datong coal obtained by using the bedding model models.

We further investigate the underlying mechanisms behind this discrepancy by adopting more realistic bedding structure, as follows.

To obtain the real bedding structure of the Datong coal, an X-ray micro CT was used to extract the 3D mesostructure of a specimen (see Fig. 9). The specimen was scanned before the SHPB test with one of the slices shown in Fig. 9a, where light color refers to higher density. It should be mentioned that higher density regions of coal is usually distributed in or close to the beddings, therefore, they can be used for estimation of the geometric distribution of the actual beddings. It is apparent that the coal has a much more complex structure that cannot be simply represented as simple single bedding plane. To directly use the CT image for model reconstruction in the DLSM is too computationally intensive (around billions of particles are required). Instead, in this work, the CT images are further processed to mimic the complex
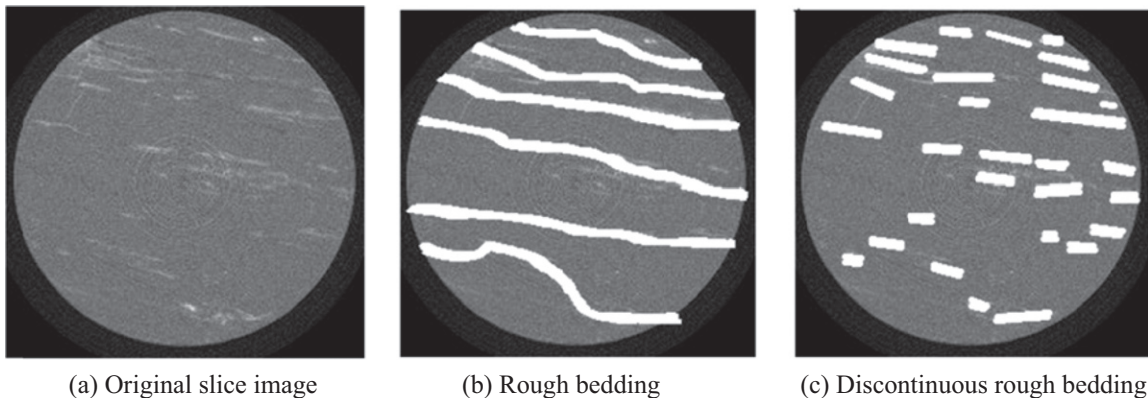

(a) Original slice image

(b) Rough bedding

(c) Discontinuous rough bedding

Fig. 9. The original CT image and artificially processed ones to represent the realistic bedding configurations in Datong coal.

(a) Rough bedding plane model
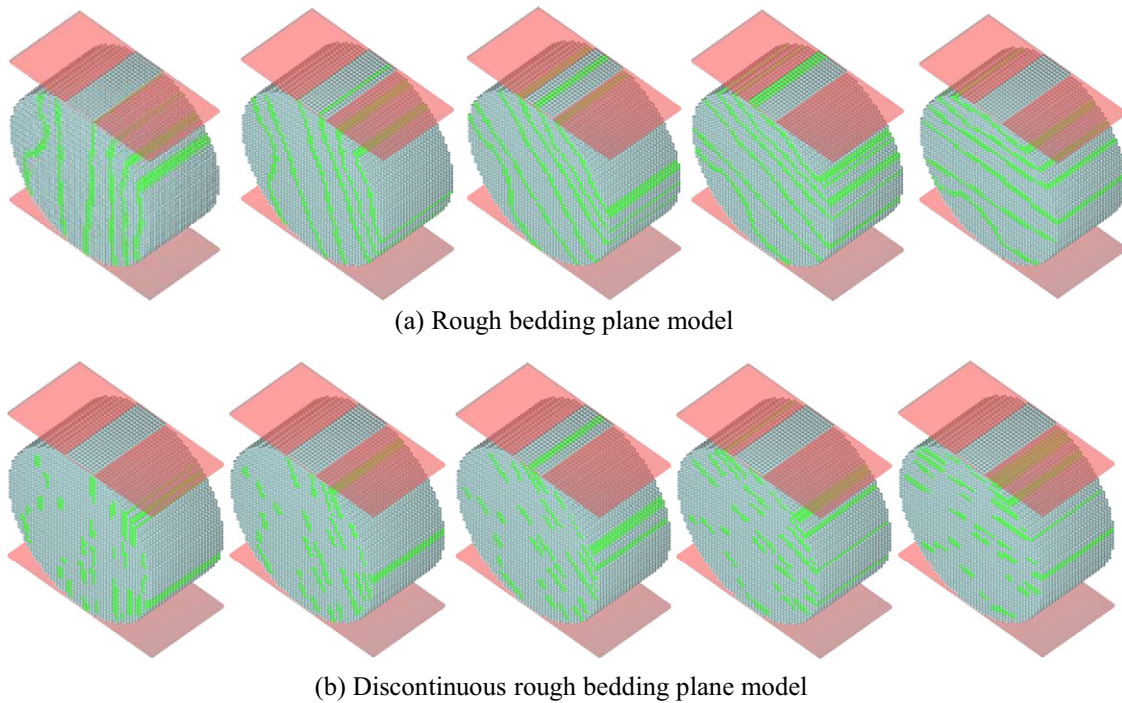

(b) Discontinuous rough bedding plane model

Fig. 10. Computational models with realistic bedding structures for the dynamic indirect tensile strength test simulated by using the DLSM.

bedding structure. As shown in Fig. 9, based on the original X-ray micro CT image, two configurations are artificially generated. One represents the coarsely-represented bedding model (Fig. 9b), and another one is the discontinuous rough-bedding model (Fig. 9c). Based on the two images and the texture mapping method (Zhao et al., 2014), the corresponding computational models are shown in Fig. 10. It should be mentioned that the bedding in the coal sample was represented artificially as a thin layer of weak material with ignoring the actual mineral properties. These beddings were sketch manually where the CT image was used as the background to help draw these irregular lines. The purpose was to have a qualitative investigation on the influence of roughness and discontinuity of the bedding on the dynamic indirect tensile strength of the coal.

The results from these numerical models are presented in Fig. 11. Compared with the bedding plane model (Fig. 12a), the rough bedding model and the discontinuous rough bedding model generate results closer to representing the influence of the bedding direction apparent in the experimental observations (see Fig. 12b–d). Therefore, both the roughness and discontinuous condition of the bedding are important in the analysis of the dynamic indirect tensile strength of Datong coal.

The failure patterns of the specimens are captured by using a high speed camera (FASTCAM SA1.1 model 675 K-CI). The image resolution is set to 384 × 352 pixels and the frame frequency is 37,500 fps (26.7 μs between two adjacent images). Fig. 12 shows the failure patterns of the coal specimens with different bedding angles predicted by the DLSM and the corresponding experimental results. The failure
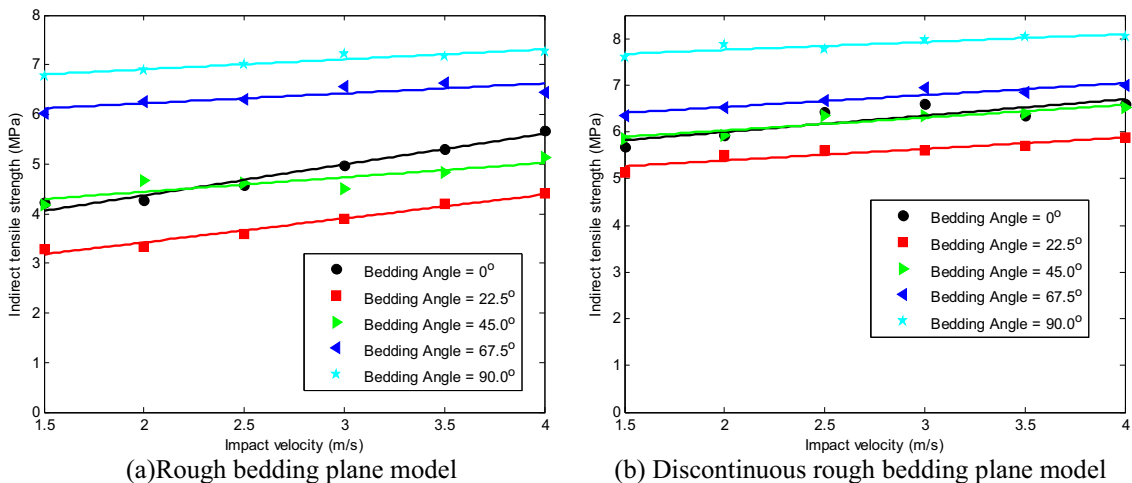

(a)Rough bedding plane model

(b) Discontinuous rough bedding plane model

Fig. 11. Dynamic indirect tensile strength versus impact velocity for Datong coal obtained by using the roughness bedding model models and discontinuous roughness bedding model models.
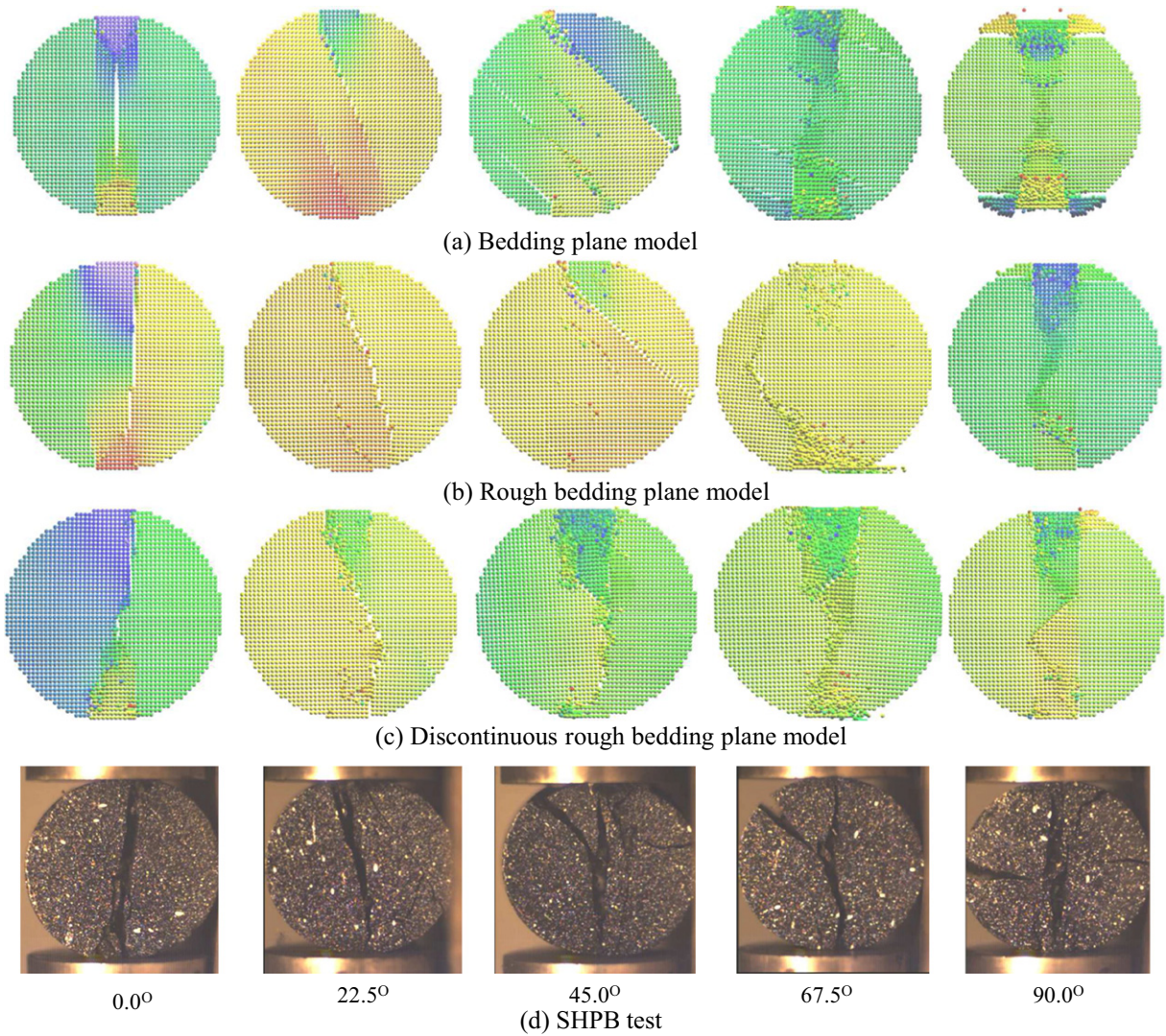
(a) Bedding plane model

(b) Rough bedding plane model

(c) Discontinuous rough bedding plane model

| 0.0º | 22.5º | 45.0º | 67.5º | 90.0º |

(d) SHPB test

Fig. 12. Failure patterns predicted by the DLSM with different bedding structures and the SHPB experimental observation.

patterns of the specimen with zero bedding angle would be the classical central line failure, with a crash zone around the loading planes. For the rest of cases, two apparent failure planes were observed, except the central failure plane, there is one additional auxiliary plane. The angle between the auxiliary plane and the main failure plane increased with the bedding angle. Again, the discontinuous rough bedding plane model produced the closest results.

From the SHPB test data and numerical simulations (see Figs. 5, 8 and 11), it is concluded that bedding direction will influence the magnitude of the dynamic indirect tensile strength. However, the difference between coal specimens with different bedding directions under the same impact velocity (loading rate) can be considered as invariant. To show this property, the strength increment (the base is the strength when bedding direction angle = 0°) versus the bedding direction are plotted in Fig. 13. The data were obtained from the fitting lines of the experimental data and numerical results in Figs. 5, 8 and 11. From Fig. 13a, it can be seen that the amplitude difference of the indirect tensile strength caused by variation of bedding direction obtained by the SHPB test is around 0.5 MPa. For numerical simulation with simple bedding, this difference is around 4.5 MPa, for the roughness model is around 4.0 MPa, and the roughness and discontinuity model is about 2.5 MPa. Based on this observation, we conclude that the roughness and discontinuity is important for the dynamic indirect tensile strength of coal.

From Fig. 13, the overall proportionality between the strength and bedding direction are apparent. To model this phenomenon, a simple linear function is introduced:

$$\Delta\sigma_t(\theta) = A\frac{\theta}{90} \tag{6}$$

where $\Delta\sigma_t(\theta)$ is the strength increment, θ is the bedding direction angle, A is the mean strength increment when $\theta = 90$ (for Datong coal $A = 0.308$ MPa).

In practical application, e.g. the development of a dynamic constitutive model for coal, the strain rate is the most commonly used variable (Xia et al., 2010). To reduce the influence of systematic errors induced into the SHPB data, the relationship between strain rate and dynamic indirect tensile strength is obtained from a linear fitting over all the experimental data (see Fig. 14). The fitting can be regarded as the dynamic indirect tensile strength function for coal specimens with a bedding direction of 45°, which is further confirmed by plotting the corresponding experimental data (Fig. 14). The linear function used to describe the dynamic indirect tensile strength of Datong coal with a bedding direction at 45° was given as

$$\sigma_t(\dot{\varepsilon}_t) = B\dot{\varepsilon}_t + C \tag{7}$$

(a) SHPB test

(b) Bedding plane model

(c) Rough bedding plane model

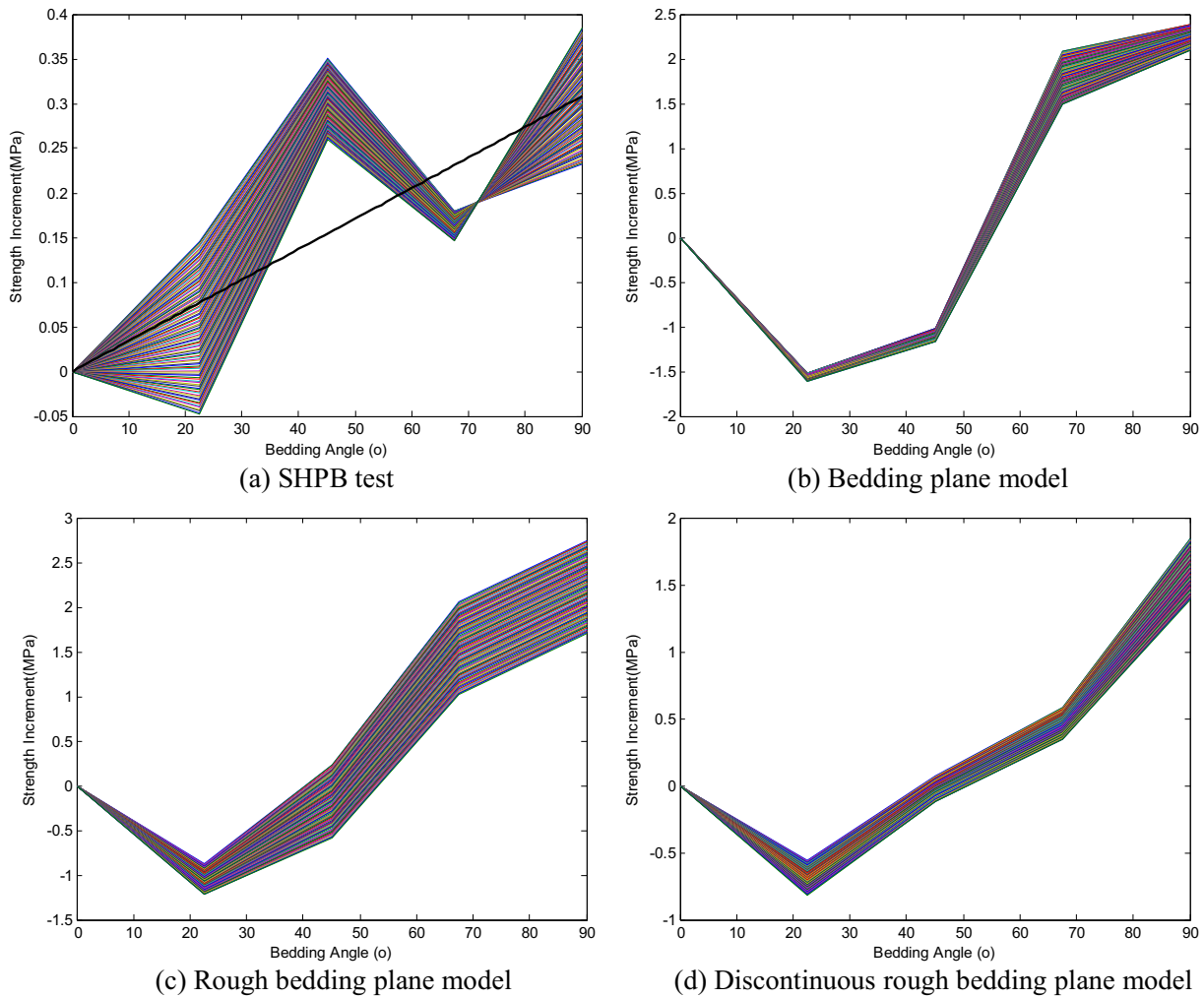(d) Discontinuous rough bedding plane model

Fig. 13. Relationships between the dynamic strength increment and bedding direction obtained from the SHPB test and the DLSM simulations.

where $\dot{\varepsilon}_t$ is the strain rate, B and C are two fitting parameters ($A = 0.0430$ MPa × s, and $B = 2.3083$ MPa for Datong coal). Substituting Eq. (6) into Eq. (7), a model considering both the dynamic effect and bedding direction for Datong coal is given as

$$\sigma_t(\dot{\varepsilon}_t) = B\dot{\varepsilon}_t + C + A\frac{2\theta-90}{90} \qquad (8)$$

in which B is a dynamic parameter, C is a strength-related parameter and A is a parameter representing the strength increment afforded by the incremented bedding direction.

4. Conclusion

In this work, the dynamic indirect tensile strength of Datong Coal is studied by using an SHPB and a discrete element based numerical modelling approach. The influence of bedding structure on dynamic strength was comprehensively studied. To explore the mechanisms by which bedding structure influences dynamic indirect tensile strength of Datong coal, the real bedding structure of a coal specimen is obtained by using a micro X-ray CT. The CT image is utilized in numerical experimentation to build an appropriate structural model and to apply dynamic analysis of failure to explore the principal influencing factors. This work shows that the dynamic indirect tensile strength of the coal is both influenced by the roughness and the continuity/discontinuity of the bedding structure. Moreover, it is observed that the dynamic

failure patterns of the coal specimen are strongly influenced by the bedding structure. Combining the SHPB data and numerical simulation, two findings are apparent. The first finding is that the impact velocity is
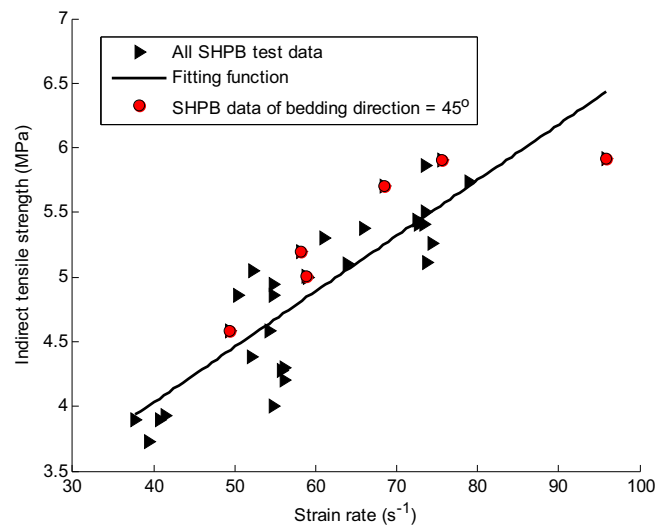

Fig. 14. Fitting function for the dynamic indirect tensile strength versus loading rate by using all data of the SHPB test.

recommended as the most critical experimental detail needed to be recorded during the SHPB test for the dynamic indirect tensile test of coal. The second finding is that the dynamic indirect tensile strength is not only influenced by the bedding direction but also by the roughness and discontinuity of the bedding. Based on these two findings, a model is developed to describe the dynamic indirect tensile strength of Datong coal.

Acknowledgments

References

ASTM D5142-09, 2009. Standard test methods for proximate analysis of the analysis sample of coal and coke by instrumental procedures. ASTM International, West Conshohocken, PA http://dx.doi.org/10.1520/D5142-09.

Dai, F., Huang, S., Xia, K., Tan, Z., 2010. Some fundamental issues in dynamic compression and tension tests of rocks using split Hopkinson pressure bar. Rock Mech. Rock. Eng. 43, 647–666.

Gong, F.Q., Zhao, G.F., 2013. Dynamic indirect tensile strength of sandstone under different loading rates. Rock Mech. Rock. Eng. http://dx.doi.org/10.1007/s00603-013-0503-7.

Kazerani, T., Zhao, G.F., Zhao, J., 2010. Dynamic fracturing simulation of brittle material using the Distinct Lattice Spring Model (DLSM) with a full rate-dependent cohesive law. Rock. Rock Eng. 43, 717–726.

Ma, G.W., Wang, X.J., Li, Q.M., 2010. Modelling strain rate effect of heterogeneous materials using SPH method. Rock Mech. Rock. Eng. 43, 763–776.

Morcote, A., Mavko, G., Prasad, M., 2010. Dynamic elastic properties of coal. Geophysics 75 (6), E227–E234.

Morgans, W.T.A., Terry, N.B., 1958. Measurements of the static and dynamic elastic moduli of coal. Fuel 37, 201–209.

Okubo, S., Fukui, K., Qi, Q.X., 2006. Uniaxial compression and tension tests of anthracite and loading rate dependence of peak strength. Int. J. Coal Geol. 68, 196–204.

Szwilski, A.B., 1984. Determination of the anisotropic elastic moduli of coal. Int. J. Rock Mech. Min. Sci. Geomech. Abstr. 21, 3–21.

Xia, K., Huang, S., Jha, A.K., 2010. Dynamic tensile test of coal, shale and sandstone using Split Hopkinson Pressure Bar: a tool for blast and impact assessment. Int. J. Geotech. Earthq. Eng. 1 (2), 24–37.

You, S., Zhao, G.F., Ji, H.G., 2011. Model for transversely isotropic materials based on Distinct Lattice Spring Model (DLSM). J. Comput. 6, 1139–1144.

Zhang, Q.B., Zhao, J., 2013. A review of dynamic experimental techniques and mechanical behaviour of rock materials. Rock Mech. Rock. Eng. http://dx.doi.org/10.1007/s00603-013-0463-y.

Zhao, J., 2000. Applicability of Mohr–Coulomb and Hoek–Brown strength criteria to the dynamic strength of brittle rock. Int. J. Rock Mech. Min. Sci. 37, 1115–1121.

Zhao, G.F., 2010. Development of micro–macro continuum–discontinuum coupled numerical method. (Ph.D thesis) EPFL, Switzerland.

Zhao, G.F., Zhao, J., 2012. Discontinuum based micromechanics methods. Proc. ICADD10 Analysis of Discontinuous Deformation,pp. 55–66.

Zhao, G.F., Fang, J., Zhao, J., 2011. A 3D distinct lattice spring model for elasticity and dynamic failure. Int. J. Numer. Anal. Methods Geomech. 35, 859–885.

Zhao, G.F., Fang, J.N., Sun, L., Zhao, J., 2013a. Parallelization of the Distinct Lattice Spring Model. Int. J. Numer. Anal. Methods Geomech. 37 (1), 51–74.

Zhao, Y., Zhao, G.F., Jiang, Y., 2013b. Experimental and numerical modelling investigation of fracturing in coal under impact loads. Int. J. Fract. 183, 63–80.

Zhao, G.F., Russell, A., Zhao, X.B., Khalili, N., 2014. Strain rate dependency of uniaxial tensile strength in Gosford sandstone by the Distinct Lattice Spring Model with X-ray micro CT. Int. J. Solids Struct. 51, 1587–1600.

Zhou, Y.X., Xia, K., Li, X.B., Li, H.B., Ma, G.W., Zhao, J., Zhou, Z.L., Dai, F., 2012. Suggested methods for determining the dynamic strength parameters and mode-I fracture toughness of rock materials. Int. J. Rock Mech. Min. Sci. 49, 105–112.

Zhu, J., Zhao, G.F., Zhao, J., Zhao, X.B., 2011. Validation study of the distinct lattice spring model (DLSM) on P-wave propagation across multiple parallel joints. Comput. Geotech. 38 (2), 298–304.

Zipf, R.K., Bieniawski, Z.T., 1990. Mixed-mode fracture toughness testing of coal. Int. J. Rock Mech. Min. Sci. 27 (6), 479–493.